The Cryosphere Discuss., 5, 1995–2033, 2011
www.the-cryosphere-discuss.net/5/1995/2011/
doi:10.5194/tcd-5-1995-2011

The Cryosphere Discussions

A three-dimensional full Stokes model of the grounding line dynamics: effect of a pinning point beneath the ice shelf

L. Favier[1], **O. Gagliardini**[1,2], **G. Durand**[1], **and T. Zwinger**[3]

[1]Laboratoire de Glaciologie et Géophysique de l'Environnement, UMR5183, UJF-Grenoble, CNRS, Saint-Martin-d'Hres, France
[2]Institut Universitaire de France, Paris, France
[3]CSC-IT Center for Science Ltd., Espoo, Finland

Received: 7 July 2011 – Accepted: 8 July 2011 – Published: 25 July 2011

Correspondence to: L. Favier (lionel.favier@lgge.obs.ujf-grenoble.fr)

Published by Copernicus Publications on behalf of the European Geosciences Union.

Abstract

The West Antarctic ice sheet is confined by a large area of ice shelves, fed by inland ice through fast flowing ice streams. The dynamics of the grounding line, i.e. the line-boundary between grounded ice and the downstream ice shelf, has a major influence on the dynamics of the whole ice sheet. However, most of the ice sheet models use simplifications of the flow equations, i.e., they do not include all the stress components, and are known to fail in their mathematical representation of the grounding line dynamics. Here, we present a 3-D full Stokes model of a marine ice sheet, in which the flow problem is coupled with the evolution of the upper and lower free surfaces, and the position of the grounding line determined by solving a contact problem between the shelf/sheet lower surface and the bedrock. Simulations are performed using the open-source finite-element code Elmer/Ice within a parallel environment. The effect of a pinning point, inserted beneath the ice shelf, on the ice dynamics is studied to demonstrate the model's ability to cope with curved and multiple grounding lines. Starting from a steady state, the sea level is slightly decreased to create a contact point between a seamount and the ice shelf. The model predicts a dramatic decrease of the shelf velocities, leading to an advance of the grounding line until both grounded zones merge together, during which an ice rumple forms above the contact area at the pinning point. Finally, we show that once the contact is created, increasing the sea level to its initial value does not cease the interaction with the pinning point and has no effect on the ice dynamics, indicating a stabilizing effect of pinning points.

1 Introduction

Most of the land ice which could contribute in the future to sea level rise belongs to Antarctica. Consequently, it is of significant relevance to investigate the amount of Antarctic ice which could be discharged from Antarctica and further contribute to sea level rise. Lately, geological observations seemed to show that the last deglaciation

TCD
5, 1995–2033, 2011

ended up with a rapid (around a century) meter-scale sea level rise, caused by ice-sheet instability (Blanchon et al., 2009). Some laser altimeter surveys carried out in West Antarctica indicated an acceleration of the ice discharge (Thomas et al., 2004), which has been confirmed recently with observations based on interferometry (Rignot et al., 2008), and also through two independent measurement techniques applied to the last 8 years (Rignot et al., 2011). In East Antarctica, the conclusion varies as it seems that the ice mass loss is near zero overall. However, stability is also questionable, because of two different sources. First, a large part of the Antarctic bedrock lies well below sea level, mainly in the West but also in a non negligible way in the East, as shown in Lythe and Vaughan (2001) and more recently with corrected data in Le Brocq et al. (2010). Moreover, from these two studies, it is also clear that the bedrock is mainly upsloping seaward near the approximative estimated location of the grounding line. The combination of these characteristics, observed also in West Antarctica, is a source of ice sheet instability, as first mentioned by Weertman (1974), since confirmed by theoretical progress (Schoof, 2007), and verified lately by numerical computations (Durand et al., 2009a).

The mass balance of marine ice-sheets is mostly controlled by the dynamics of the transition zone between the grounded ice-sheet and the floating ice-shelf, around the grounding line. Mechanically, grounded ice is mainly both vertically and sideways sheared, while floating ice is mainly longitudinally stretched and sideways sheared. These different stress components are superimposed within the vicinity of the grounding line, resulting in a complex stress pattern involving all components. This complexity is difficult to represent numerically. Until 2005, as demonstrated by Vieli and Payne (2005), none of the numerical models available properly described the grounding line migration. The fourth assessment of IPCC (Solomon et al., 2007) also pointed out that dynamical effects in marine ice sheets were badly understood, and badly represented in models.

Our lack of understanding of marine ice sheet dynamics comes from two aspects: the degree of complexity resolved by the numerical models, and the grid in which velocity

TCD
5, 1995–2033, 2011

solutions are computed. The most complete models resolve the full Stokes set of equations without any approximations in the stress tensor (Durand et al., 2009a). So far, this approach has not really been applied to the grounding line migration issues, a crucial reason coming from huge CPU time computation which has to be overcome, even if some attemps have been made in 2-D by Lestringant (1994), then more recently by Nowicki and Wingham (2008), Durand et al. (2009a) and Gagliardini et al. (2010). The reason is that a highly refined grid is required at the transition between grounded ice and floating ice (Durand et al., 2009b), i.e., around the grounding line, whether the grid is fixed or moving. A moving grid needs a fewer number of elements because the refined part of the mesh and the grounding line migrate altogether, which helps the computational time comparatively with fixed grids. These high numerical costs are increasingly addressed by using computational clusters with parallel computations. All the other models are more or less based on asymptotical approximations of the Stokes equations. The simplest of these models are based on the so-called Shallow Ice Approximation (SIA), initially developed in Hutter (1983), in which only vertical shear components are considered. The SIA is valid for a small aspect ratio between domain thickness and length, but not where the basal sliding contribution to the ice dynamics increases, or where the basal surface slope is too steep (Le Meur et al., 2004), like in the vicinity of the grounding line. More complex models were also developed, such as those including higher order stress gradients (Pattyn, 2003; Saito et al., 2003), but these models neglect the resistive stress, whereas at the transition zone between grounded and floating ice, this term should be accounted for. Some models also adopt an SIA approach for the grounded ice where shearing dominates the flow, and a Shallow Shelf Approximation (SSA, MacAyeal, 1989) for the floating ice where stretching dominates.

Some models take into account a curved grounding line in a 3-D geometry, as in Pattyn (2003) where the shelf is modeled, or in Katz and Worster (2010) where the shelf is replaced by a flux at the grounding line, computed from asymptotic theories from Schoof (2007), but not represented physically. However, little attention has been

TCD
5, 1995–2033, 2011

paid numerically on the effect of a pinning point touching the ice basal surface and creating a localized grounded zone surrounded by floating ice, except in Goldberg et al. (2009) in which an SIA-SSA coupled model is used. These pinning points are known to stabilize marine ice sheets (Fricker et al., 2009), and have been detected in Antarctica beneath the Ross and the Amery ice shelves.

In this study, we present a 3-D numerical model based on a full-Stokes approach of a marine ice-sheet, in which none of the stress components are neglected. We are mainly interested in the mechanical effects, and temperature is assumed uniform and constant. The model is largely inspired from the work done by Durand et al. (2009a), and extended to the 3-D case. The ice flows down from a symmetric ice divide towards a calving front. Vertically, the ice body is bounded by two surfaces, the upper stress free ice/air interface, and the lower interface in contact with either the sea or the bedrock. The evolution of these surfaces is determined by solving a local transport equation. The grounding line position results from the resolution of a contact problem, and is therefore fully part of the solution. Because of the 3-D geometry, the ice is also bounded sideways by two lateral walls for which perfect sliding is prescribed. The purpose of this paper is mostly to present the model and its ability to represent correctly the behaviour of curved and multiple grounding lines in 3-D. To do so, we applied the model to a pinning point experiment, from which we obtained these grounding lines. The model described above was implemented within the open source finite element code Elmer (downloadable at www.csc.fi/elmer).

A general description of the model is provided in Sect. 2, followed by an overview of the model algorithm in Sect. 2.5 in which we explain how we resolve the position of the grounding line. The model is validated in Sect. 3 by demonstrating its reversibility. The dynamical effect of a pinning point in contact with the ice shelf basal surface is then investigated in Sect. 4. Finally, some conclusions about the ability of the model to represent curved and multiple grounding lines are discussed.

TCD
5, 1995–2033, 2011

2 Detailed description of the model

Using the finite element code Elmer/Ice in 3-D, we solve the problem of a gravity-driven flow of isothermal, incompressible and nonlinear viscous ice, which slides over a rigid bedrock. The grounding line, which separates the floating and the grounded part of the ice, falls into fixed grid points and migrates according to the solution of a contact problem.

2.1 Geometry and main hypothesis

The geometry of the marine ice sheet is three-dimensional and the mesh is composed of 8-nodes linear brick elements. It includes a grounded part that slides over a rigid bedrock and a floating part, the grounding line being the boundary between these two domains. The main direction of the flow is aligned with the x axis, the z axis is the vertical pointing upwards, and the transversal y axis is perpendicular to the (x,z) plane (see Fig. 1 for geometry details). The domain is bounded transversally by two lateral boundaries, both parallel to the (x,z) plane. The ice divide ($x = 0$) is considered to be a symmetry axis and the length of the ice sheet remains similar over time, which means that the calving front has a fixed position throughout the simulation.

The constitutive law for the ice behaviour follows a Norton-Hoff type law (also named Glen's flow law in glaciology)

$$\boldsymbol{S} = 2\eta \boldsymbol{D}, \tag{1}$$

where $\boldsymbol{S}$ is the deviatoric stress tensor, and $\boldsymbol{D}$ the strain rate tensor, whose components are defined by

$$D_{ij} = \frac{1}{2}\left(\frac{\partial u_i}{\partial x_j} + \frac{\partial u_j}{\partial x_i}\right), \tag{2}$$

TCD
5, 1995–2033, 2011

where $\boldsymbol{u}$ is the velocity vector. The effective viscosity η is expressed as

$$\eta = \frac{1}{2} A^{-1/n} \dot{\varepsilon}_e^{(1-n)/n}, \tag{3}$$

where $\dot{\varepsilon}_e$ is the second invariant of the strain rate defined as

$$\dot{\varepsilon}_e^2 = \frac{1}{2} D_{ij} D_{ij}. \tag{4}$$

In Eq. (3), A is the fluidity parameter, kept constant since ice is assumed to be isothermal (see Table 1), and Glen's flow law exponent is $n = 3$.

2.2 Governing equations

To determine the ice flow velocities and pressure, we solve the full Stokes equations over the ice volume, consisting in the momentum conservation equations without inertial effects:

$$\mathrm{div}\boldsymbol{\sigma} + \rho_i \boldsymbol{g} = 0, \tag{5}$$

and the mass conservation equation in case of incompressibility:

$$tr\boldsymbol{D} = div\boldsymbol{u} = 0. \tag{6}$$

In Eq. (5), $\boldsymbol{\sigma} = \boldsymbol{S} - p\boldsymbol{I}$ is the Cauchy stress tensor with $p = -tr\boldsymbol{\sigma}/3$ the isotropic pressure, ρ_i the ice density and $\boldsymbol{g}$ the gravity vector.

The three-dimensional ice body is vertically limited by two free surfaces, namely the top interface $z = z_s(x,y,t)$ between ice and air, and the bottom interface $z = z_b(x,y,t)$ between ice and bedrock or sea (see Fig. 1). A local transport equation is solved to determine the evolution of the two free interfaces; its general form is:

$$\frac{\partial z_j}{\partial t} + u_x \frac{\partial z_j}{\partial x} + u_y \frac{\partial z_j}{\partial y} - u_z = a_j, \tag{7}$$

TCD
5, 1995–2033, 2011

where u_x, u_y, u_z are functions depending on the triplet (x,y,z_j), and z_j and a_j depend on the triplet (x,y,t). The subscript j can refer either to the upper interface ($j=s$) or to the lower interface ($j=b$), $u_x(x,y,z_j)$ and $u_y(x,y,z_j)$ are the velocities in the horizontal plane for the considered interfaces, and $a_j(x,y,t)$ is the accumulation/ablation function. Here, the accumulation a_s over the upper interface is a downward vertical flux uniform and constant, while the melting/accretion a_b below the ice shelf is neglected (see Table 1).

2.3 Boundary conditions

2.3.1 Ice divide

At $x=0$, the ice divide is assumed to be a symmetry axis, so that the prescribed velocity is $u_x(0,y,z)=0$.

2.3.2 Ice front

The end of the domain where the shelf ends, the so-called calving front, keeps a constant position. If sufficiently large, the distance between the calving front and the grounded ice has no influence on the upstream flow dynamics, since no friction is accounted for on the lateral boundaries.

The front boundary undergoes a normal stress due to the sea pressure $p_w(z,t)$ evolving vertically as:

$$p_w(z,t) = \begin{cases} \rho_w g(l_w(t)-z), & z < l_w(t) \\ 0, & z \geq l_w(t) \end{cases} \quad (8)$$

where ρ_w is the sea density and l_w the sea level. The stress imposed is thus $\sigma_{nn}=p_w$ and $\sigma_{nt}=0$.

TCD
5, 1995–2033, 2011

2.3.3 Upper interface

The atmospheric pressure exerted against the upper interface $z = z_s(x,y,t)$ is neglected, which implies that $\sigma_{nn}|_s = \boldsymbol{n}\cdot(\sigma\cdot\boldsymbol{n})|_s = 0$, and $\sigma_{nt}|_s = \boldsymbol{t}\cdot(\boldsymbol{\sigma}\cdot\boldsymbol{n})|_s = 0$, where $\boldsymbol{n}$ is the unit normal vector of the interface pointing outward, $\boldsymbol{t_1}$ and $\boldsymbol{t_2}$ the unit tangent vectors of the interface.

2.3.4 Lower interface

The lower interface $z = z_b(x,y,t)$ may be in contact with either the sea or the bedrock, so two kinds of boundary conditions coexist inside a unique surface. Where the bottom surface is in contact with the sea, the sea pressure is applied with no shearing, which means that:

$$\begin{cases} \sigma_{nt}|_b = 0 \\ \sigma_{nn}|_b = p_w(z,t) \end{cases} \tag{9}$$

Where the bottom surface is in contact with the bedrock, a non linear friction law is prescribed, which is summarized as:

$$\begin{cases} \sigma_{nt}|_b = C|\boldsymbol{u}\cdot\boldsymbol{t}|^{m-1}(\boldsymbol{u}\cdot\boldsymbol{t}) \\ \boldsymbol{u}\cdot\boldsymbol{n} = 0 \end{cases} \tag{10}$$

where the values of the parameters C and m entering the friction law are given in Table 1.

2.3.5 Lateral walls

The lateral boundaries of the domain are parallel planes. The first plane ($y = 0$) is an actual border of the domain, and the second one ($y = w$) corresponds to a symmetry axis. In both cases, no flux is considered through the surfaces and the boundary

TCD
5, 1995–2033, 2011

condition prescribed is $u_y(x,0,z) = u_y(x,w,z) = 0$. The model gives us the possibility to prescribe a non linear friction law, like the one discussed above in Eq. (10). This possibility will not be explored in this paper and perfect sliding is assumed.

2.4 General considerations for the mesh

One of the conclusions of the fourth assessment of IPCC (Solomon et al., 2007) was that dynamical effects in ice sheets were badly understood, and badly represented in models. For the particular case of full Stokes models, the reason lies principally in the mesh size adopted around the grounding line. Durand et al. (2009a) came to the conclusion that a refinement within tens of meters was necessary to yield consistent results, even if the neutral equilibrium, a numerical artefact in 2-D (Schoof, 2007), could not be removed completely for any of these experiments. We use also a full Stokes model so we anticipated this issue, by taking care to use the recommended value of tens of meters to minimize the impact of the mesh size on the dynamics. Because our simulations were carried out in 3-D, we had to compromise when choosing a mesh size around the grounding line. This paper further presents numerical transient computations of the grounding line moving through tens of kilometers. Therefore, because we use a fixed grid, a fine mesh was adopted wherever the grounding line is expected to migrate.

The procedure for building the mesh is twofold. A 2-D steady state is first computed, then laterally extruded in the y-direction, and finally relaxed during a century to guarantee that the perturbation experiments start from a fully steady state geometry. This procedure is much faster than growing a marine ice sheet in 3-D from an initial slab of uniform thickness.

2.5 Model algorithm

A simplified algorithm of the model is presented in Fig. 2. The first step, carried out once at the beginning of the simulation, is to give the model a geometry with a related mesh, plus initial pressure and velocity fields.

TCD
5, 1995–2033, 2011

The following step is to initialize the basal boundary condition. As already mentioned, two different boundary conditions coexist within the lower surface, Dirichlet conditions where velocity is prescribed and Neumann conditions where a load integrated from the hydrostatic pressure is prescribed. A node defined by its coordinates (x_i, y_i, z_i) is floating if $z_b(x_i, y_i, t) > b(x_i, y_i)$ and grounded if $z_b(x_i, y_i, t) = b(x_i, y_i)$.

Then, the model enters the first loop of the simulation. An important first step is to compute the nodal force F_w exerted by the sea, on the floating or grounded ice. This is done by integrating the sea pressure (see Eq. 8) over the element boundary faces according to the shape function.

The discretisation and linearisation of the full Stokes equations by the finite element method leads to a linear system in the form of $\boldsymbol{A} \cdot \boldsymbol{X} = \boldsymbol{b}$, with $\boldsymbol{b}$ a four-component vector, three for velocity plus one for the pressure, times the number of nodes. The non-Newtonian stress-strain relationship introduces nonlinearities into the problem, and the previous linear system adopts the nonlinear form of $\boldsymbol{A}(\boldsymbol{X}) \cdot \boldsymbol{X} = \boldsymbol{b}(\boldsymbol{X})$. This nonlinear system is linearized to the form $\boldsymbol{A}(\boldsymbol{X}_{i-1}) \cdot \boldsymbol{X}_i = \boldsymbol{b}(\boldsymbol{X}_{i-1})$ and solved with direct methods, and the numerical solution is stabilized using the residual free bubbles method (Baiocchi et al., 1993). The convergence criterion of the nonlinear system is based on the change in the Euclidian norm of the solution between the $(i-1)^{\text{th}}$ and the i^{th} iterations. Convergence is first reached when this criterion falls below 10^{-3}, assuming a fixed grounding line at the position calculated during the previous time step.

Then the contact between grounded nodes and the bedrock is tested. If the contact force R (computed from the residual of the Stokes system, see Durand et al. (2009a) for more details) exerted by the ice on the bedrock falls below the force exerted by the sea F_w, the concerned node is no longer under Dirichlet conditions but undergoes the sea pressure (see Fig. 3). This change in the basal conditions leads to a retreat of the grounding line. The finite element problem is thus altered by the change in the boundary condition. This time, the convergence of the nonlinear system is pushed further to 10^{-5}, assuming this new basal boundary condition.

TCD
5, 1995–2033, 2011

As mentioned before, Eq. (7) is solved to adjust the lower and upper surfaces. Technical and numerical details on the method are explained in Gagliardini and Zwinger (2008). The following update of vertical surface positions requires to check whether the difference between the bedrock and the ice lower surface evolves. At this stage, some floating nodes may be reattached to the bedrock following the condition already mentioned above.

The type of boundary condition assigned to a node on the lower ice surface is represented by a mask that takes the value 1 for a grounded node and −1 for a floating node. Those nodes defining the grounding line are then identified as grounded points with at least one floating neighbour (see Fig. 4). To those points the value of 0 is assigned in the mask.

3 Validation of the 3-D full Stokes model

The following experiment is to validate the model. It is about the insertion of a pinning point below the ice shelf to create a new grounded area, in the middle of floating ice. After a century, the pinning point is artificially removed and the simulation pushed further until the model reaches again a steady state. The removal of the pinning point makes the bedrock uniform in the y-direction, which can be seen as a 2-D extruded geometry. In that case, we know from the previous work done by Schoof (2007) that only one steady state exists, so the grounding line should go back to its initial position. However, from the previous work done by Durand et al. (2009b), we expect an offset between the initial and the final steady states.

3.1 Description of the pinning point experiment

The bedrock is composed of a linear surface and a gaussian surface, and defined by (in meters):

$$z = b(x,y) = \max(\, b_{\text{lin}} \,;\, b_{\text{gaus}} \,), \tag{11}$$

TCD
5, 1995–2033, 2011

with

$$\begin{cases} b_{\text{lin}} = -100 - x/1000 \\ b_{\text{gaus}} = 541.2 \times \exp\left(\frac{-(x-563000)^2-(y-50000)^2}{2\times 10000^2}\right) - 1000, \end{cases} \quad (12)$$

which corresponds to a linear downsloping bedrock with a superimposed 3-D gaussian curve acting as a pinning point (see Fig. 5).

The initial steady state is obtained by applying the parameters given in Table 1. In order to optimise the computational time, we take the advantage of the longitudinal symmetry plane such that only half of the domain width is accounted for in the computation. The summit of the gaussian bump is located about 0.8 m below the ice basal surface. At this stage, only one grounding line exists, it is perpendicular to the (x,z) plane and located at $x_{gi} = 536.8$ km. At the beginning of the simulation, the sea level is instantaneously lowered by 1 m, which creates rapidly (within one time step) a contact between the gaussian bump and the ice basal surface, at the position $(x,y) = (563.50)$ in km, about 27 km downstream the initial grounding line. Then the geometry evolves during a century with the same configuration. After 100 years, the sea level is increased back to its initial value and the gaussian bump is simply removed to release the corresponding contact. Following these operations, only one grounding line remains. Of course, the abrupt change in the bedrock geometry has no geological reasons, but it allows us to test the reversibility of the model. The simulation is then continued to reach a new steady state with a fully stabilized grounding line, obtained after 600 years.

3.2 Mesh and partitioning

The maximum refinement chosen for areas in the vicinity of the grounding line is 50 m in the x-direction, whereas the grid size in the y-direction is constant and equals to 2.5 km. This high refinement has to be applied to the whole area where the grounding line is expected to pass, which means from the initial grounding line to the newly created grounded zone around the pinning point, over around 30 km. As a consequence, we

TCD
5, 1995–2033, 2011

end up with a large amount of mesh nodes: a little under 800 nodes in the x-direction, 21 nodes in the y-direction and 11 nodes in the z-direction, which corresponds to about 180 000 nodes. To optimise the CPU time, this mesh is broken down into 48 partitions, each consisting of about 4000 nodes (see Fig. 6).

3.3 Advance and retreat of the grounding line

Figure 7 shows the migration of the grounding line during the whole experiment. Figure 8 shows the vertically averaged velocities in the x-direction for two flowlines, at $y = 0$ km and at $y = 50$ km at the location of the bump, for both the initial and final steady states, and for the last time at which the pinning point is in contact ($t = 100$ a).

The new contact created between the ice and the bump leads to a decrease of the velocities between both grounded areas (see Fig. 7b) and at the initial grounding line. Since the accumulation is constant on the upper surface, the grounded volume increases (see Fig. 9) and the initial grounding line advances towards the pinning point (see Fig. 7a). This advance takes place in a nearly linear way for each y-coordinate, and curves with more advance directly upstream the top of the bump, where velocities decrease the most (see Fig. 8). After 100 years, the grounding line has undergone a 3 km advance at $y = 0$ km and a slightly more than 5 km advance at $y = 50$ km.

After 100 years, the pinning point is removed and the sea level recovers its initial value. The grounding line retreats until a new steady state is reached. Its final position is about 1.5 km downstream its initial position, but the velocity at the grounding line is nearly similar to its initial value despite this offset. As already explained above, the position of the grounding line depends on the maximum refinement considered around this particular area. This issue was already highlighted in Durand et al. (2009a), from which we know that this offset is not related to the initial advance, therefore if we had simulated a greater advance, the offset would nonetheless have been similar. Moreover, the curvature of the grounding line under the influence of the pinning point completely vanishes so it recovers its initial straight shape.

TCD
5, 1995–2033, 2011

In conclusion, despite a slight offset in the reversibility of the grounding line migration, we have sufficient confidence in our model to keep on using it for ice sheet modelling. We are aware that the mesh size has an effect on the dynamics but take care of using a small enough mesh size at the grounding line to control and limit these effects.

4 Mechanical irreversibility of the pinning point experiment

4.1 Description of the experiments

Two kinds of simulations are carried out here (summarized in Table 2). The first experiment (called pp exp) is similar for the first hundred years to the previous one presented in Sect. 3. The difference is that the pinning point is not released and the sea level keeps constant at −1 m. Then the geometry evolves during nearly a thousand years. The second experiment (called back exp) is to increase the sea level back to its initial level of 0 m, without any change in the bedrock, so the pinning point still exists. The purpose is to check if the insertion of a contact point with the lower ice surface induces any mechanical irreversibility of the ice flow dynamics.

4.2 Results of the experiment pp exp

After the first 100 years (similar to the validation experiment, in Section 3.3), the grounding line still advances (see Fig. 10) and the global volume of the ice sheet still grows (see Fig. 9) until both grounded areas merge together, after around 900 years of simulation (a similar result was obtained by Goldberg et al. (2009) with a SSA model). The main grounding line is rapidly curved under the effect of a non uniform velocity along the y-direction. This is because along the symmetry axis (where the bump stands), the velocity field is lower than along the wall (at $y = 0$ km). This means that the influence of this supplementary amount of friction below the ice has more influence directly upstream the pinning point. This is confirmed in Fig. 11 which shows

TCD
5, 1995–2033, 2011

velocities around grounding lines along the flowlines $y = 0$ km and $y = 50$ km. At the main grounding line upstream the top of the bump, the velocity is about 50 % lower than along the wall.

Figure 12 represents the position of the main grounding line at $y = 0$ km (in dashed black line) and $y = 50$ km (in solid black line), and the x-extremal positions of the grounding line at the pinning point for $y = 50$ km. The advance rate of the main grounding line is fast in the first place, and then slows down in the second part of both curves. The meeting between both grounded areas takes place at around 800 years. It is followed by oscillations of the last grounded point, which is due to the fact that the grounding line lies on an upsloping part of the bedrock, well known source of instability in marine ice sheets (Schoof, 2007). This instability stops after 1000 years after which only one grounded zone remains.

At the beginning of the simulation, the last grounded point (blue curve in Fig. 11), which belongs to the grounding line part of the pinning point, retreats from its position at the top of the bump, towards the main grounding line. The pinning point actually grows and migrates upstream. This is certainly induced by the decrease of the velocity upstream the new contact below the shelf, which may increase the efficiency of the sea pressure downstream and could cause this retreat. This migration adopts a linear profile during the first 100 hundred years, to stop at a nearly stable position, around 5 km upward from its initial position, under the effect of the sea pressure on both sides of the pinning point.

Figure 13 shows 3-D views ($t = 0$, 100, 500, 900 a) of the modeled marine ice sheet around grounding line areas. Longitudinal deviatoric stresses are superimposed to geometries. At the main grounding line, the ice undergoes a longitudinal tensile stress, which can be explained by the friction gap from positive to 0 when moving seaward around the grounding line. This is immediately followed seaward by a stress oscillation, which is also observed inside the ice. A similar behaviour is observed at the secondary grounding line which belongs to the pinning point. This tensile behaviour is counterbalanced by a compressive behaviour between both grounded zones, before

TCD
5, 1995–2033, 2011

they meet. It is also due to the gap between basal friction properties. At the end of the simulation, when both grounded areas merge into one, it seems that this compressive behaviour disappears. This corresponds to the fact that the intermediate floating zone becomes completely grounded, which removes the intermediate gap in the basal friction.

The downstream shift between compressive and tensile behaviours forms an ice rumple on the upper surface. Its geometry is more or less stable between 100 a and 900 a of simulation and its presence is closely related to the presence of the pinning point, which creates this stress field. The ice rumple is 50 m high, which represents one tenth of the ice shelf thickness. It is vertically aligned with the position of the basal pinning point, and both extend over a similar horizontal distance of around 3 km.

4.3 Results of the experiment back exp

The second experiment is to increase the sea level back to 0 m, its initial value, close to the beginning of the experiment pp exp, at $t = 1.5$ a. The bedrock keeps the bumped part in contact with the ice lower surface. Figure 9 also shows the volume over time for this experiment (in green line). The curve development is parallel to the blue one at slightly lower values, which shows that the contact between the pinning point is not released. This happens at the very beginning of the simulation so we expect it to continue throughout the following time steps.

To explain the irreversibility, we plotted in Fig. 14 the minimum critical value of sea level rise sl_{eq} that would be required to release this contact. Its value is computed for the grounded lower surface of ice by the formula:

$$sl_{eq} = \frac{\sigma_{nn} - \rho_w g(l_w - z))}{\rho_w g}. \quad (13)$$

This parameter corresponds to the difference between the normal stress undergone by the ice surface and the sea pressure, normalised by $\rho_w g$, to interpret it in terms of sea level equivalent.

TCD
5, 1995–2033, 2011

Note that a few of the sl_{eq} values are negative for the more advanced part of both grounding lines. There, the sea load against the ice is higher than the contact load exerted by the ice on the bedrock, indicating that these nodes are about to detach from the bedrock.

It turns out that, even after only 1.5 a of the experiment pp exp, the value of sl_{eq} is already high. To remove the contact between the seamount and the ice lower surface, it would be necessary to rise the sea level by more than 20 m. This is clearly an irreversibility induced by the presence of the new contact with the seamount in the middle of the shelf.

After 1.5 a, the contact with the seamount below the shelf extends over no more than 300 m. Afterwards, during a transition period of 100 a, already described and shown in Fig. 12, this contact area migrates upward and grows to finally extend over 3 km. Until the merge between both grounded areas, this zone keeps the same position and size. During this time period, the value of sl_{eq} equals nearly instantaneously one half of the value taken after 100 years. This means that a new formed pinning point below the shelf leads very rapidly to a configuration where the ice sheet grows in volume whatever the further physically acceptable increase that would be applied to the sea level.

5 Conclusions

Motivated by the lack of knowledge about dynamical effects within marine ice sheets, particularly when the transversal direction is considered, we modeled the grounding line dynamics in 3-D using the finite element code Elmer/Ice. This new model is an evolution of a 2-D model previously developed in Durand et al. (2009a). The 3-D full Stokes velocity field is computed and coupled with the evolution of both the ice-air and the ice-bedrock/sea interfaces. Using this model, the dynamics of the ice sheet are taken into account without the common approximations of the Stokes equations. The algorithm of the finite element model was presented in order to highlight the fact that grounding line retreat and advance are treated separately. The retreat is the possible

TCD
5, 1995–2033, 2011

result of a contact problem, evaluated by the deviation of the ice overburden from integrated sea water pressure. The advance is based on the geometrical comparison between altitudes, and is a result of the lower free surface evolution.

We investigated the capacity of the model to generate acceptable advance and retreat of the grounding line. To do so, we generated an initial 3-D steady state of a marine ice sheet with a straight grounding line uniform in the y-direction. Then, a seamount was added to the bedrock, its top located less than one meter below the ice shelf, at slightly more than 25 km downstream the initial grounding line. Then the sea level was decreased by 1 m to create a contact with the seamount. After 100 years, the seamount was simply removed, the sea level increased back to its initial level, and a new steady state was reached. After 100 years in this simulation, the main grounding line was curved, it had advanced by 3 to 5 km, and the maximum advance was directly upstream the pinning point. The back experiment led to a retreat of the grounding line to reach a position 1.5 km ahead of the initial grounding line, and the curvature had completely disappeared. This offset in the position was expected since we know from the literature that full Stokes models are dependent on the mesh size at the grounding line (Durand et al., 2009b). However, compromises were made to limit and control this issue, as a maximum mesh refinement of 50 m was applied to the model.

Then, we pushed this pinning point experiment beyond 100 a until more than 1000 a. Along with the volume increase of the ice sheet, the model predicts that the advance of the main grounding line leads after 800 a to a merge between both grounded areas. The advance rate is the highest in the same flowline as the pinning point, which is due to a higher decrease of the velocities. The newly created contact with the pinning point, first located at the top of the seamount, migrates upstream with a constant velocity during the first 100 a. Then it adopts a stable position on the upsloping part of the seamount until both grounding lines meet.

Longitudinal tensile stress was highlighted at the main grounding line and at the secondary grounding line which belongs to the pinning point. Within the floating areas between both grounded areas, the behaviour is on the contrary compressive. This is

TCD
5, 1995–2033, 2011

due to a shift in the basal friction between grounded and floating ice, where the friction is null. This shift between longitudinal compressive and tensile stresses is particularly apparent at the vertical of the pinning point, where it forms an ice rumple on the top surface. The ice rumple and the pinning point have a similar size in the (x, y) plane, and they are located on top of each other. The height of the ice rumple is about one tenth of the ice shelf thickness.

Finally, whether the ice sheet is likely to detach from the pinning point when the sea level is increased back to its initial value. The model predicts that even if the sea level increase occurs at the very beginning of the simulation, the contact with the pinning point is not released. After further investigation based on a comparison between normal stress and sea pressure for the grounded ice, it turned out that the necessary increase of the sea level to remove the pinning point would be at least 20 times the initial decrease. This shows that a pinning point plays a stabilising role on the marine ice sheets, even if the contact may have lasted only a few years.

The mesh resolution is a crucial issue for proper modeling of grounding line and marine ice sheet dynamics. The finer the mesh at the grounding line, the more precise its position and therefore the better the prediction of marine ice sheet dynamics. Compromises have to be done in the mesh size to bound under acceptable CPU time simulations. However, the use of moving mesh techniques, which allows the maximum refinement to move along with the grounding line, can help us to decrease the mesh resolution as only the areas displaying high gradients are meshed with the finest grid.

While Schoof's flux boundary condition (Schoof, 2007) is beginning to be used by the glaciological community (Pollard and DeConto, 2009), it is important to test its validity for more complex ice sheet/ice shelf problems, particularly when the ice mass evolves in a transient state within a non fully stabilized geometry. The model presented here is ready to be used to carry out such studies. Melting and buttressing can be considered physically, and the bedrock topography can be modified to simulate real geometries, so a longer-term perspective will be to apply the model to a real Antarctica drainage basin.

TCD
5, 1995–2033, 2011

Acknowledgements. This work was supported by funding from the ice2sea programme from the European Union 7th Framework Programme, grant number 226375. Ice2sea contribution number 043. Computations presented in the paper were performed at the CSC – IT Center for Science (Finland) and at the Centre Informatique National de l'Enseignement Supérieur (CINES, France). The authors would like to thank the efficient assistance given by the Elmer developers.

The publication of this article is financed by CNRS-INSU.

References

Baiocchi, C., Brezzi, F., and Franca, L.: Virtual bubbles and Galerkin-least-squares type methods (Ga. LS), Comput. Method. Appl. M., 105, 125–141, 1993. 2005

Blanchon, P., Eisenhauer, A., Fietzke, J., and Liebetrau, V.: Rapid sea-level rise and reef backstepping at the close of the last interglacial highstand, Nature, 458, 881–884, 2009. 1997

Durand, G., Gagliardini, O., De Fleurian, B., Zwinger, T., and Le Meur, E.: Marine ice sheet dynamics: Hysteresis and neutral equilibrium, J. Geophys. Res., 114, 10 pp., F03009, doi:10.1029/2008JF001170, 2009a. 1997, 1998, 1999, 2004, 2005, 2008, 2012

Durand, G., Gagliardini, O., Zwinger, T., Le Meur, E., and Hindmarsh, R.: Full Stokes modeling of marine ice sheets: influence of the grid size, Ann. Glaciol., 50, 109–114, 2009b. 1998, 2006, 2013

Fricker, H., Coleman, R., Padman, L., Scambos, T., Bohlander, J., and Brunt, K.: Mapping the grounding zone of the Amery Ice Shelf, East Antarctica using InSAR, MODIS and ICESat, Antarct. Sci., 21, 515–532, 2009. 1999

Gagliardini, O. and Zwinger, T.: The ISMIP-HOM benchmark experiments performed using

TCD
5, 1995–2033, 2011

the Finite-Element code Elmer, The Cryosphere, 2, 67–76, doi:10.5194/tc-2-67-2008, 2008. 2006
Gagliardini, O., Durand, G., Zwinger, T., Hindmarsh, R., and Le Meur, E.: Coupling of ice-shelf melting and buttressing is a key process in ice-sheets dynamics, Geophys. Res. Lett., 37, L14501, 5 pp., doi:10.1029/2010GL043334, 2010. 1998
Goldberg, D., Holland, D., and Schoof, C.: Grounding line movement and ice shelf buttressing in marine ice sheets, J. Geophys. Res, 114, 23 pp., F04026, doi:10.1029/2008JF001227, 2009. 1999, 2009
Hutter, K.: Theoretical glaciology: material science of ice and the mechanics of glaciers and ice sheets, Springer, 1983. 1998
Katz, R. and Worster, M.: Stability of ice-sheet grounding lines, Proceedings of the Royal Society A: Mathematical, Physical and Engineering Science, 466, 1597, 2010. 1998
Le Brocq, A., Payne, A., and Vieli, A.: An improved Antarctic dataset for high resolution numerical ice sheet models (ALBMAP v1), Earth System Science Data, 2, 247–260, 2010. 1997
Le Meur, E., Gagliardini, O., Zwinger, T., and Ruokolainen, J.: Glacier flow modelling: a comparison of the Shallow Ice Approximation and the full-Stokes solution, C. R. Phys., 5, 709–722, 2004. 1998
Lestringant, R.: A two-dimensional finite-element study of flow in the transition zone between an ice sheet and an ice shelf, Ann. Glaciol., 20, 67–71, 1994. 1998
Lythe, M. and Vaughan, D.: BEDMAP: A new ice thickness and subglacial topographic model of Antarctica, J. Geophys. Res., 106(B6), 11335–11351, doi:10.1029/2000JB900449, 2001. 1997
MacAyeal, D.: Large-scale ice flow over a viscous basal sediment- Theory and application to ice stream B, Antarctica, J. Geophys. Res., 94, 4071–4087, 1989. 1998
Nowicki, S. and Wingham, D.: Conditions for a steady ice sheet-ice shelf junction, Earth Planet. Sci. Lett., 265, 246–255, 2008. 1998
Pattyn, F.: A new three-dimensional higher-order thermomechanical ice sheet model: Basic sensitivity, ice stream development, and ice flow across subglacial lakes, J. Geophys. Res, 108, 10–1029, 2003. 1998
Pollard, D. and DeConto, R.: Modelling West Antarctic ice sheet growth and collapse through the past five million years, Nature, 458, 329–332, 2009. 2014
Rignot, E., Bamber, J., Van den Broeke, M., Davis, C., Li, Y., Van de Berg, W., and Van Mei-

TCD
5, 1995–2033, 2011

jgaard, E.: Recent Antarctic ice mass loss from radar interferometry and regional climate modelling, Nat. Geosci., 1, 106–110, 2008. 1997

Rignot, E., Velicogna, I., van den Broeke, M., Monaghan, A., and Lenaerts, J.: Acceleration of the contribution of the Greenland and Antarctic ice sheets to sea level rise, Geophys. Res. Lett., 38, 5 pp., L05503, doi:10.1029/2011GL0465832011, 2011. 1997

Saito, F., Abe-Ouchi, A., and Blatter, H.: Effects of first-order stress gradients in an ice sheet evaluated by a three-dimensional thermomechanical coupled model, Ann. Glaciol., 37, 166–172, 2003. 1998

Schoof, C.: Ice sheet grounding line dynamics: Steady states, stability, and hysteresis, J. Geophys. Res, 112, 19 pp., F03S28, doi:10.1029/2006JF000664, 2007. 1997, 1998, 2004, 2006, 2010, 2014

Solomon, S., Qin, D., Manning, M., Marquis, M., Averyt, K., Tignor, M. M. B., LeRoy Miller, H., and Chen, Z.: Climate change 2007: the physical science basis, Cambridge University Press Cambridge, 2007. 1997, 2004

Thomas, R., Rignot, E., Casassa, G., Kanagaratnam, P., Acuña, C., Akins, T., Brecher, H., Frederick, E., Gogineni, P., Krabill, W., Manizade, S., Ramamoorthy, H., Rivera, A., Russell, R., Sonntag, J., Swift, R., Yungel, J., and Zwally, J.: Accelerated sea-level rise from West Antarctica, Science, 306, 255, 2004. 1997

Vieli, A. and Payne, A.: Assessing the ability of numerical ice sheet models to simulate grounding line migration earth surface, J. Geophys. Res., 110, 18 pp., F01003, doi:10.1029/2004JF000202, 2005. 1997

Weertman, J.: Stability of the junction of an ice sheet and an ice shelf, J. Glaciol., 13, 3–11, 1974. 1997

TCD
5, 1995–2033, 2011

Table 1. Numerical values of the parameters adopted for the simulations.

Parameter	Symbol	Value	Units
Fluidity parameter	A	10^{-25}	$\mathrm{Pa}^{-3}\,\mathrm{s}^{-1}$
Seconds per year		31 536 000	$\mathrm{s\,a}^{-1}$
Accumulation rate	a_s	0.5	$\mathrm{m\,a}^{-1}$
Melting/accretion	a_b	0	$\mathrm{m\,a}^{-1}$
Glen's exponent	n	3	
Bed friction parameter	C	10^{7}	$\mathrm{Pa\,m}^{-1/3}\,\mathrm{s}^{1/3}$
Bed friction exponent	m	1/3	
Sea density	ρ_w	1000	$\mathrm{kg\,m}^{-3}$
Ice density	ρ_i	900	$\mathrm{kg\,m}^{-3}$
Gravity constant	g	9.81	$\mathrm{kg\,m}^{-3}$
Domain length	L	800	km
Domain half width	w	50	km
Maximum refinement		50	m

TCD
5, 1995–2033, 2011

Table 2. Summary fo the experiments carried out and their characteristics. The experiment back exp starts from the experiment pp exp after $t = 1.5$ a.

Experiment	Sea level (m)	Pinning point	Start (a)
pp exp	−1.0	exists	0
back exp	0.0	exists	1.5

TCD
5, 1995–2033, 2011

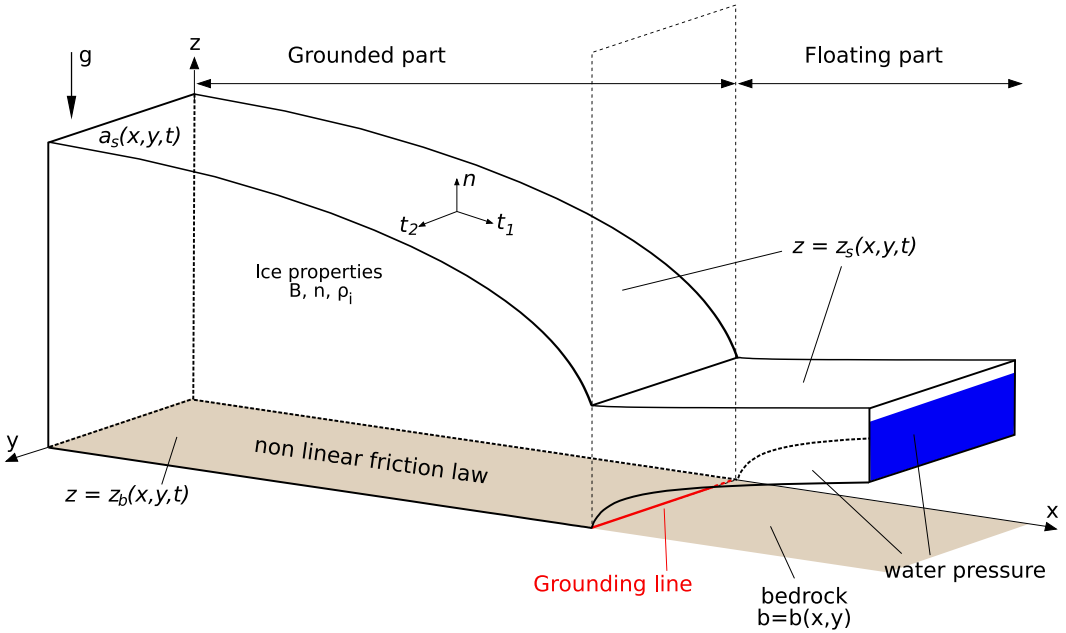

Fig. 1. Main characteristics of the modelled geometry.

TCD
5, 1995–2033, 2011

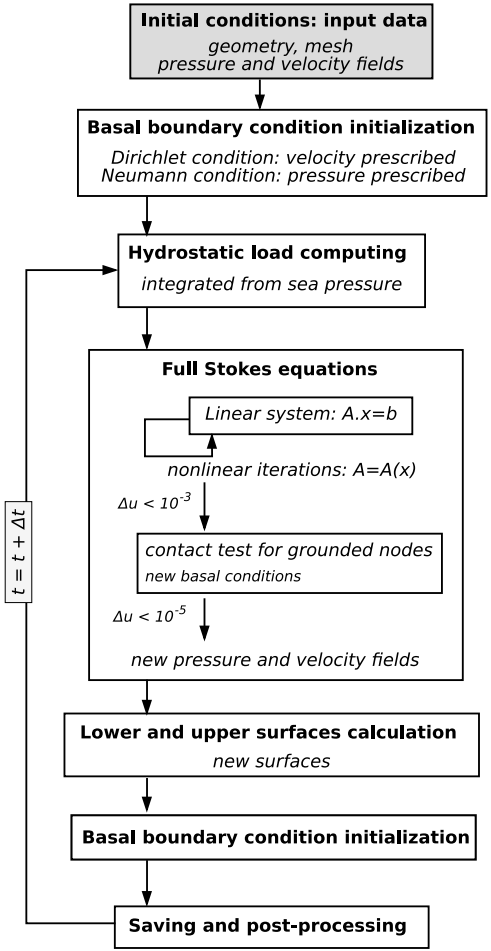

Fig. 2. Simplified algorithm of the model.

TCD
5, 1995–2033, 2011

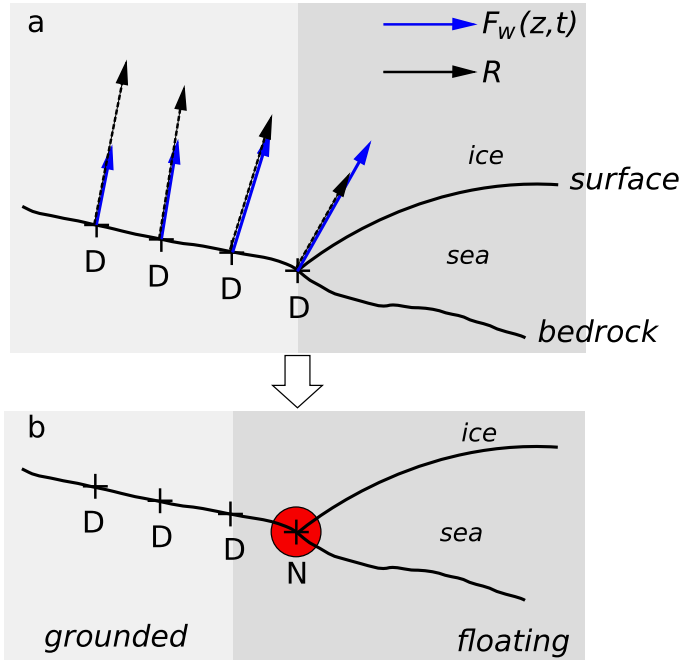

Fig. 3. Main retreat process of the grounding line, which takes place when the convergence criterion of the Stokes nonlinear system falls below 10^{-3}. For a grounded node, if the sea load is higher than the ice/bedrock contact force **(a)**, then this node (red circle) becomes floating for the rest of the Stokes system convergence **(b)**. Boundary conditions prescribed: N for Neumann and D for Dirichlet.

TCD
5, 1995–2033, 2011

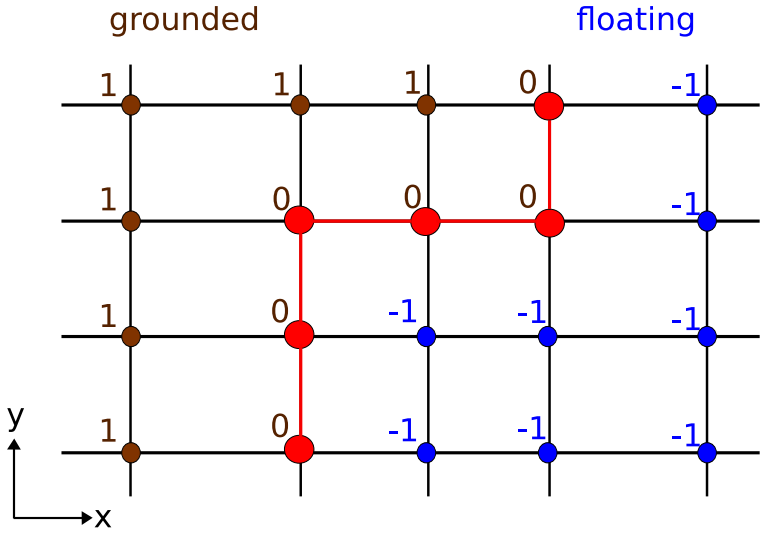

Fig. 4. Part of the bedrock mesh (projection on the (x, y) plan) with floating nodes (-1 in blue), grounded nodes (1 in brown). The grounding line nodes (0 in red) correspond to grounded nodes located at the boundary between floating and grounded nodes.

TCD
5, 1995–2033, 2011

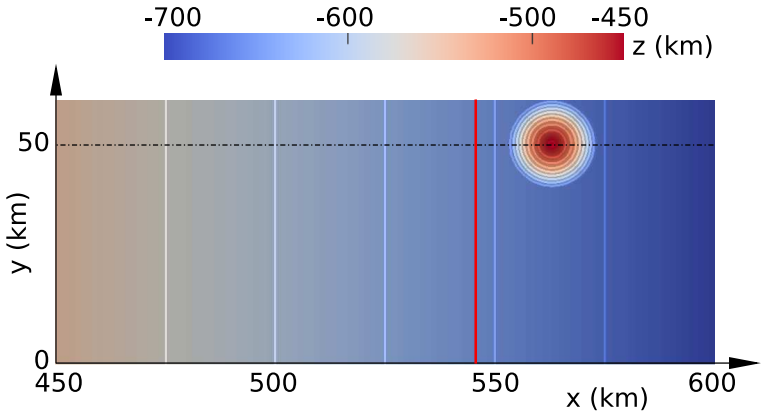

Fig. 5. Top view of the bedrock geometry (zoom around the initial grounding line and the bump), consisting of a linear area and a gaussian bump. Altitude isovalues are displayed every 25 m. The symmetry axis is shown by the dashed line.

TCD
5, 1995–2033, 2011

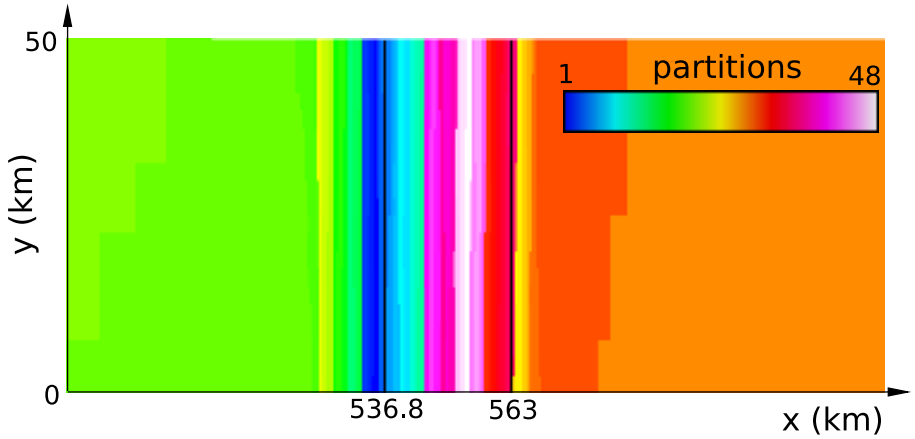

Fig. 6. Geometry partitioning related to parallel computations (zoom around the initial grounding line and the bump). Each of the 48 partitions consists of approximately 4000 nodes.

TCD
5, 1995–2033, 2011

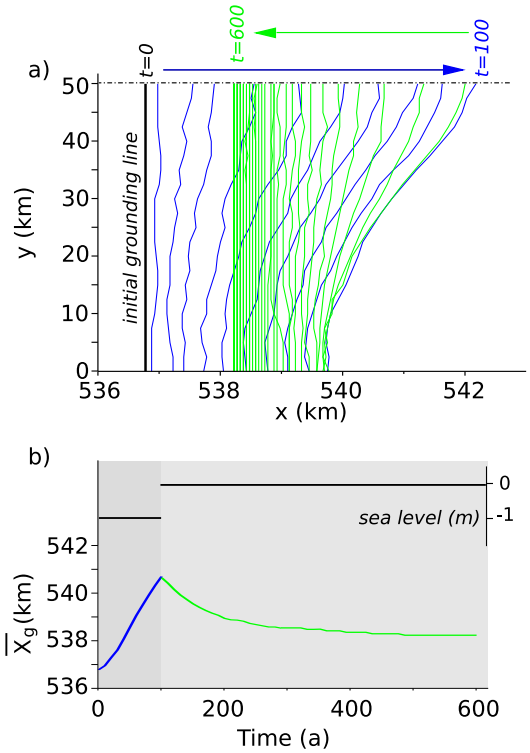

Fig. 7. Migration of the grounding line over time. The contact between the pinning point and the ice lasts 100 years, then the contact is removed. Advance and retreat processes are shown in blue and green respectively. **(a)** Top view in the (x, y) plane. **(b)** Averaged position of the initial grounding line. The new grounding line created at the pinning point is not shown here.

TCD
5, 1995–2033, 2011

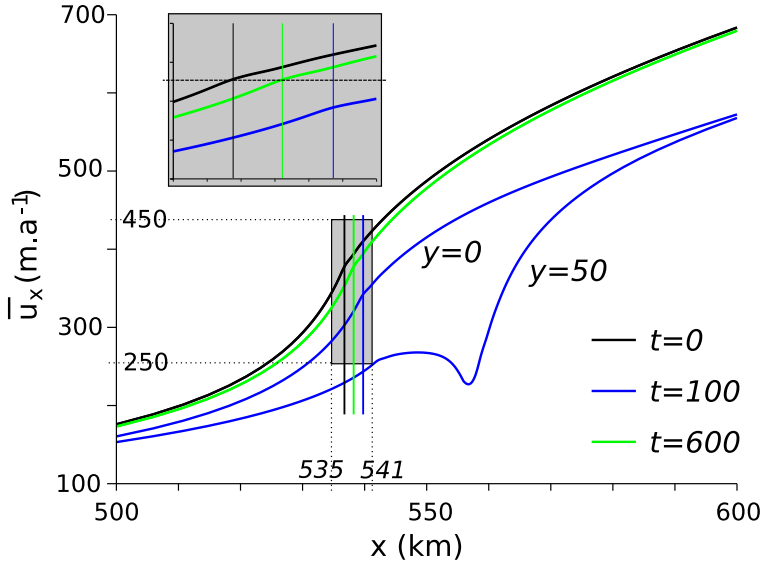

Fig. 8. Vertically averaged velocity in the x-direction $\bar{u}_x$ along x for $t = 0$ a (steady state without the contacting pinning point, in black), $t = 100$ a (last point in time with the pinning point, in blue), and $t = 600$ a (new steady state 500 a after the removal of the pinning point, in green). The position of the grounding line for each point in time is shown by the vertical lines. The inset is an enlargement of the grey part. A horizontal dashed line is plotted to highlight the similarity of velocities between initial and final steady states at the grounding line.

TCD
5, 1995–2033, 2011

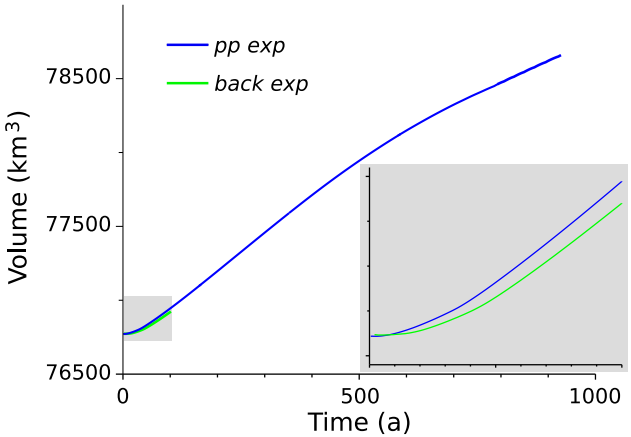

Fig. 9. Evolution over time of the ice volume for the pinning point experiment (blue curve), and the reversibility experiment (green curve). The inset is a zoom into the first 100 years.

TCD
5, 1995–2033, 2011

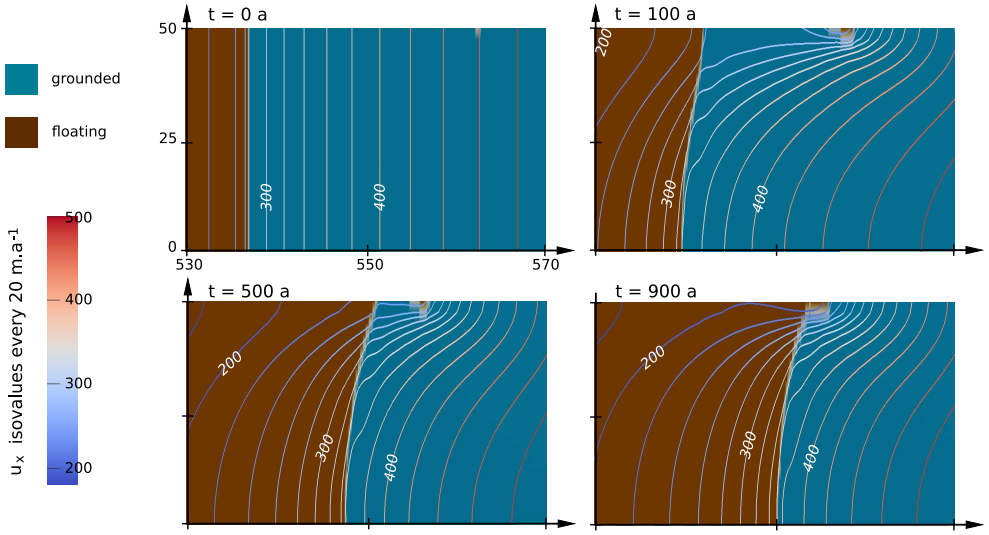

Fig. 10. Effect of the pinning point on the grounding line migration, for a few time-levels between 0 and 900 years of simulation. Basal velocity norm isovalues are also represented every 20 m a^{-1}, and displayed every 100 m a^{-1} for clarity.

TCD
5, 1995–2033, 2011

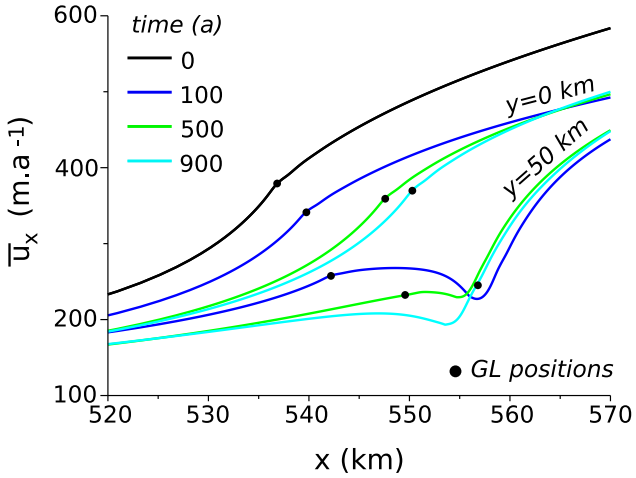

Fig. 11. Effect of the pinning point on the vertically integrated velocity $\bar{u}_x$. Depicted profiles are along the symmetry axis $y = 50$ km and along the lateral wall $y = 0$ km, for $t = 0$, 100, 500, 900 years of simulation. The position of the grounding line for similar y-coordinate is also shown.

TCD
5, 1995–2033, 2011

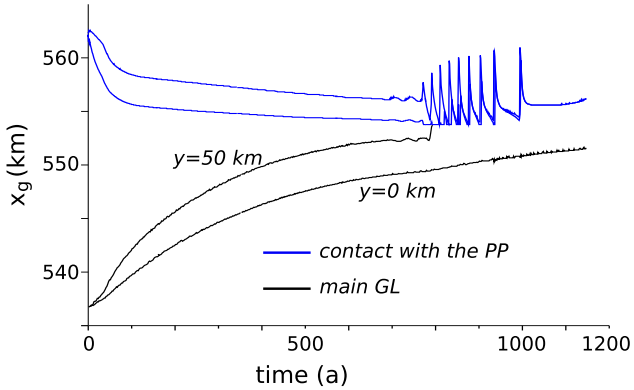

Fig. 12. Positions of grounding lines over time. The main grounding line is shown for $y = 0$ km in dashed black line, and for $y = 50$ km in solid black line. The first and the last grounded points of the pinning point for $y = 50$ km are shown in solid blue lines.

TCD
5, 1995–2033, 2011

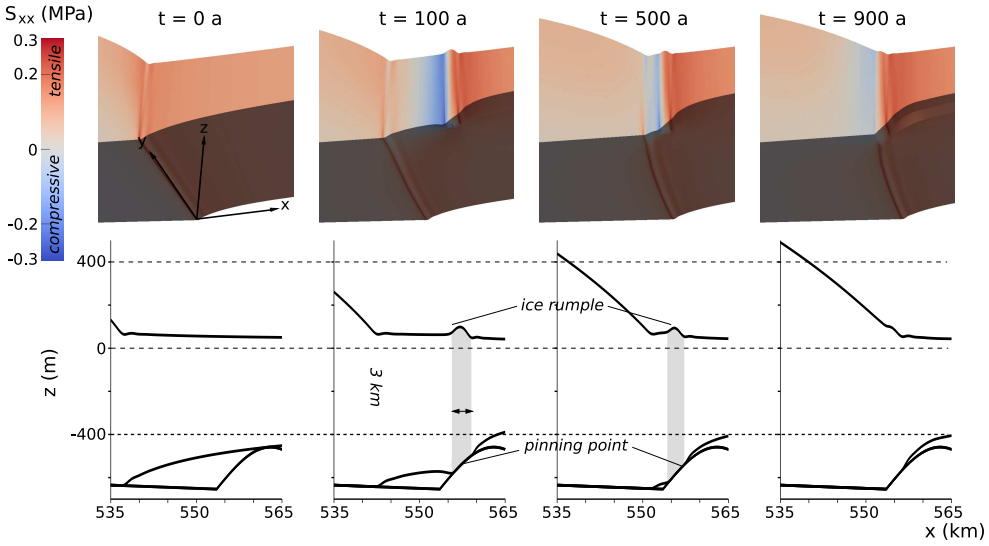

Fig. 13. Geometrical evolution over time (after $t = 0, 100, 500, 900$ years into the simulation) for the pinning point experiment, superimposed with the longitudinal deviatoric stresses (top series). View in the (x, z) plane of the flowline $y = 50$ km (bottom series). An ice rumple forms on the upper surface under the effect of the contact between the pinning point and the ice lower surface. Both are vertically aligned all over the simulation until both grounded parts merge together.

TCD
5, 1995–2033, 2011

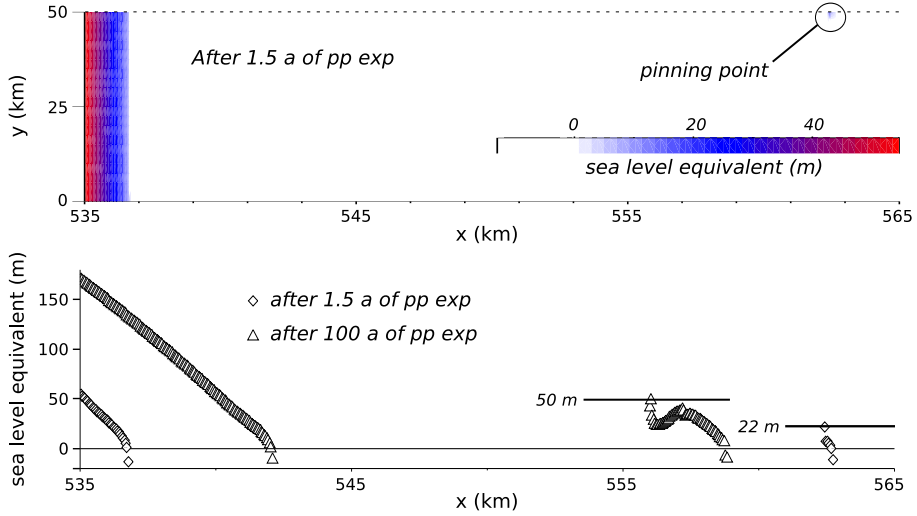

Fig. 14. Difference between normal stress and sea pressure in terms of sea level rise equivalent at the beginning of the pinning point experiment, at $t = 1.5$ and 100 a. (top) 2-D view around the grounding line areas. (bottom) Along the flowline $y = 50$ km, only the grounded points are represented. Horizontal lines represent the sea level rise to impose on the model to release the pinning point.

TCD
5, 1995–2033, 2011